2019 IEEE 15th International Conference on Automation Science and Engineering (CASE)

Neural-Network-Based Heart Motion Prediction for Ultrasound-Guided Beating-Heart Surgery

Lingbo Cheng[a, *], *student member, IEEE*, and Mahdi Tavakoli[a], *member, IEEE*

[a]*Department of Electrical and Computer Engineering, University of Alberta, Edmonton, AB, T6G 1H9, Canada*

***Abstract*-A neural-network-based heart motion prediction method is proposed for ultrasound-guided beating-heart surgery to compensate for time delays caused by ultrasound (US) image acquisition and processing. Such image processing is needed for tracking heart tissue in US images, which is itself a requirement for beating-heart surgery. Once the heart tissue is tracked in US images, a recurrent neural network (NN) is employed to learn how to predict the motion of the tracked heart motion in order to compensate for the delays introduced in the initial US image processing step. To verify the feasibility of predicting both simple and complex heart motions, the NN is tested with two types of heart motion data: (i) fixed heart rate and maximum amplitude, and (ii) varying heart rate and maximum amplitude. Also, the NN was tested for different prediction horizons and showed effectiveness for both small and large delays. The heart motion prediction results using NN are compared to the results using an extended Kalman filter (EKF) algorithm. Using NN, the mean absolute error and the root mean squared error between the predicted and the actually tracked heart motions are roughly 60% smaller than those achieved by using the EKF. Moreover, the NN is able to predict the heart position up to 1000 ms in advance, which significantly exceeds the typical US image acquisition/processing delays for this application (160 ms in our tests). Overall, the NN predictor shows significant advantages (higher accuracy and longer prediction horizon) compared to the EKF predictor.**

I. Introduction

Robotic-assisted beating-heart surgery has significant advantages over the arrested-heart surgery such as reducing the risk of cognitive loss, decreasing the recovery time, and enabling intraoperative evaluation of the heart [1]. Without the assistance of a surgical robot, it is super difficult for the surgeon to operate on a beating heart as the velocity and acceleration of it are approximately 210 mm/s and 3800 mm/s^2, respectively [2]. Therefore, developing a robot to automatically compensate for the heart's motion is the focus of current research in the medical robotics community [3]–[6]. With a robotic-assisted beating-heart surgical system, the surgeon would have a feeling of operating on an "arrested" heart as the surgical robot can be controlled to synchronize itself with the beating heart's motion.

*Corresponding Author.
E-mails: lingbo1@ualberta.ca, mahdi.tavakoli@ualberta.ca.

The robotic assistance approaches for beating heart's motion compensation can be divided into three major categories: (a) force-based method, (b) impedance-based method, and (c) position-based method. In [7], [8], the authors implemented different control approaches to reject disturbances caused by the heart's motion so that the contact force between the surgical instrument and the heart tissue can be kept to a desired value. The constant contact guarantees the beating heart's motion is well compensated for.

As a generalization of the above approaches, impedance-based methods [3], [5] control the dynamic behaviour between the surgical robot and the heart instead of treating the surgical robot and the heart as isolated systems. The beating heart can be regarded as a disturbance to the surgical robot, and the disturbance response of the surgical robot can be modulated to control the dynamic behaviour between the surgical robot and the heart by changing the parameters and/or structure of the impedance [9]. For instance, in [3], a reference impedance model for the surgical robot was designed to be flexible to make sure the surgical robot comply with the heart's motion.

The above methods require the surgical instrument to keep in contact with the heart tissue all the time. Once the contact disappears, they are not going to achieve the motion compensation goal. In this case, the best approach would be based on position control. For position-based motion compensation methods, several types of sensors have been used to capture the position of the heart such as high-speed camera, X-ray and CT, infrared radiometer, magnetic resonance imaging, and US machine. Considering the requirements for visualization of the interior of the beating heart (i.e. seeing through the blood) and the safety, economy and convenience of use of the sensors, US imaging is the most appropriate choice for heart tissue tracking.

In [6], [10], the authors obtained the position of a point of interest (POI) on the heart from US images and used position to control on the surgical robot so that it follows the motion of the heart. However, the time delay caused by US image acquisition and processing is non-negligible and has to be compensated for. Otherwise, the position control loop of the surgical robot will not be able to make the robot's motions synchronized to the heart motions; instead, the robot will follow the delayed heart motions, which creates the risk of the surgical robot puncturing the heart due to a collision.

978-1-7281-0355-6/19/$31.00 ©2019 IEEE

To compensate for the time delay, the delayed POI position should be predicted. Such a heart motion prediction is a problem of time series forecasting, which required a model to predict future values of the time series based on its present and previously observed values. Various methods have been proposed to solve time series forecasting problems such as Kalman filtering, weighted moving average, and exponential smoothing. As the heart motion is quasi-periodic, in our previous work [4], an extended Kalman filter (EKF) was used for motion prediction. To improve the prediction accuracy, in this paper, a neural network (NN)-based heart motion prediction method is proposed. It has been demonstrated that a NN model can approximate any continuous function and it has been successfully used for forecasting of many time series in many applications [11]–[14]. Also, NN has the advantage that it can approximate nonlinear functions without any prior information of the data series, which makes it suitable for application of quasi-periodic beating-heart motion prediction.

Much of the past work [14]–[16] on using NN to predict an organ's physiological motion has focused on radiotherapy and the prediction of tumor motion under respiration. For image-guided radiotherapy applications, diagnostic X-ray imaging was used to detect the markers on the tumor. Different from these works, in this paper, US imaging is used to obtain the POI position and no markers are implanted on the surface of the heart to reduce the harm to the human body and increase the observation accuracy of the POI position.

For the NN model, there are different architectures that can be chosen such as feedforward NN and recurrent NN for the time series forecasting problems. The main difference between the feedforward and recurrent NNs is the presence of feedback loops in the latter network. The presence of feedback loops in the recurrent NN has a profound positive impact on the learning capability and on the prediction performance. Therefore, a recurrent NN is used in the paper. To verify its ability to predict heart motion data, two types of datasets are acquired: (i) fixed heart rate and maximum amplitude, and (ii) varying heart rate and maximum amplitude. Also, different prediction horizons are tested. A schematic of the proposed steps is shown in Fig. 1. A US machine acquires images of a beating heart and a surgical instrument and passes the image sequences to the image processing algorithms to capture the POI position. The heart tissue position data is then fed to a recurrent NN for training it to predict the heart motion. The last step involves evaluating the performance of the NN.

To the best knowledge of the authors, this is the first research on using recurrent NN to predict POI position for US image-guided beating-heart surgery. The rest of the paper is organized as follows. Section II introduces the approach for POI motion tracking in US images. Section III presents the NN based motion prediction method. Section IV shows the results of using the NN algorithm and compares them to those of using the EKF algorithm. Section V concludes the paper.

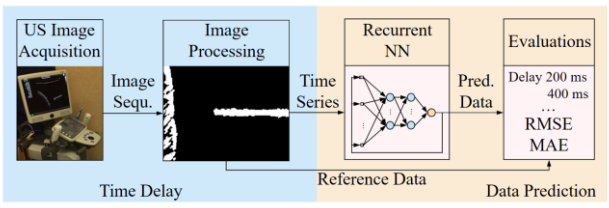

Figure 1. A schematic of the propsed steps for heart motion prediction.

II. Heart Motion Tracking

The time series of beating-heart motion data can be obtained through the acquisition and processing of a sequence of US images showing the beating heart. As discussed later, the position of the POI on the beating heart is defined as the heart position along the surgical instrument's axis, and it can be calculated through feature extraction algorithms. When the surgical instrument is kept still, the POI position can be acquired directly from the measured tool-heart distance along the surgical tool's axis.

A. Image Acquisition

The US image sequences are acquired through a 6MHz 4dl14-5/38 linear 4D transducer connected to a SonixTouch US scanner (SonixTouch from Ultrasonix, Richmond, BC, Canada) (Fig. 2). The 2D US images are collected from the US scanner using a DVI2USB 3.0 frame grabber (Epiphan, Ottawa, ON, Canada). The frame rate of the US scanner is 25 Hz. A one-degree-of-freedom custom-built mechanical cam and a voice coil actuator (NCC20-18-020-1X from H2W Technologies Inc., Santa Clarita, CA, USA) are used to simulate the beating heart's motion. The heart simulator can produce motion signals, which temporally matched to an ECG signal [17], with a peak-to-peak amplitude of 9 mm. At the tip of the heart simulator, an artificial plastisol-based tissue is mounted on to simulate the heart tissue. A straight and rigid tool is used as the surgical instrument. Both the plastic tissue and the rigid tool are submerged in a water tank to simulate the heart's blood pool and guarantee that they are visible under the US. The depth of the US images is 5.5 cm.

B. Image Processing

To capture the heart motion data, each US image frame is first converted to a binary image by choosing a threshold of 0.3. Then, a 3×3 Sobel edge detection and a Hough transform are used to obtain, respectively, the edge points and the longest line (as the detected surgical tool). The extension of the longest line intersects the edge of the heart tissue, and the

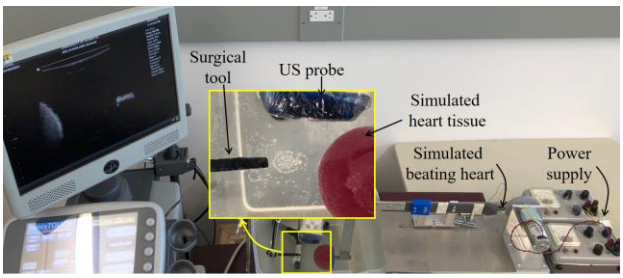

Figure 2. The experimental setup for US image acquisition.

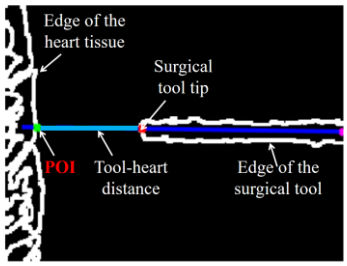

Figure 3. The detected tooltip, POI, and tool-heart distance.

intersection point is considered as the POI (Fig. 3).

The tracked POI position in the image frame is converted to the world coordinate by converting it from pixels into mm, and the time series of the POI position is obtained (Fig. 4a). To compare the tracked POI position data with the simulated heart's directly measurable position, a potentiometer (LP-75FP-5K from Midori America Corp., Fullerton, CA, USA) is used to collect and record the real-time position of the beating-heart simulator. The mean absolute error between the tracked data and the directly measured data of a 1000 s-long data is 0.5697 mm, which is 0.0633 of the peak-to-peak amplitude of the heart motion and is sufficiently small.

Five US image sequences each ~ 1000 s long are recorded for the training and test of the NN. The corresponding time series of the tracked POI position data are labelled as dataset 1-5. These data are approximately periodic as the simulated heart keeps creating the same motions, which means the fundamental frequency (f_1 = 1.12 Hz) and the maximum amplitude of the motions are fixed (Fig. 4b).

To further simulate more realistic and complex heart motion, the voltage applied to the voice coil actuator of the simulated heart, which is responsible for creates the back-and-forth motion, is changed. Also, the maximum amplitude of the simulated heart motion is changed by using springs of different stiffnesses in the heat simulator, thus changing how closely the simulator's end point follows the motions of the rotating cam. Five similar 1000 s long US image sequences are recorded and the time series of the acquired POI position data are labelled as dataset 6-10. The power spectral density (PSD) of the POI position data show that the dominant peaks are f_{21} = 0.8214, f_{22} = 1.123, and f_{23} = 1.310 Hz (Fig. 4b).

To implement the NN, the acquired ten POI position

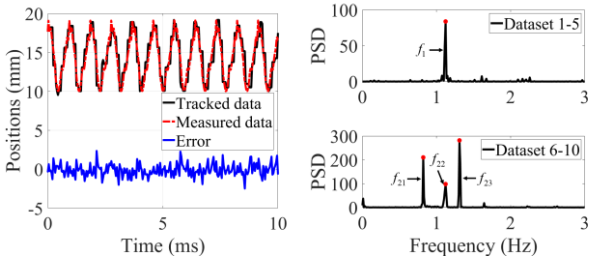

(a) (b)

Figure 4. (a) Time series of the tracked and directly measured POI position with fixed heart rate and amplitude. (b) The PSDs of the tracked POI position captured from two types of US image sequences.

datasets will be split into training and out-of-sampling test subsets, separately. Specifically, the first 75% of each dataset is used for training and the left is reserved for testing.

III. Heart Motion Prediction

For training the NN that will predict the heart motion, the tracked heart motion $x(n)$ serves both as the input and the output or the observation (albeit with the difference that the former is delayed with respect to the latter). The prediction problem can, therefore, be described as given an input vector $\mathbf{x}(n)$, the NN model must capture the underlying dynamics responsible for generating $x(n+1)$ as shown in Fig. 5. For multiple-step ahead prediction of $x(n)$, namely, to predict $x(n+D)$, where D is the delay length that needs to be compensated for, a closed-loop nonlinear autoregressive (NAR) network is employed as discussed later.

A. Recurrent NN

A recurrent NN is a class of NN where connections between units form a directed cycle. In other words, it has at least one feedback loop. The advantage of a recurrent NN is it can use its internal memory to process sequences of inputs. In this paper, as the problem is to predict the quasi-periodic heart motion $x(n)$ which is a time series given the present and past values of $x(n)$, there is no external input to the network, a NAR network, therefore, is appropriate to learn and implement the recursive prediction of heart motion.

The architecture layout of a NAR is shown in Fig. 6, which employs a generic recurrent NN that follows naturally from a static multilayer perceptron (MLP) with two hidden layers. The NAR model has a single output that is fed back to the

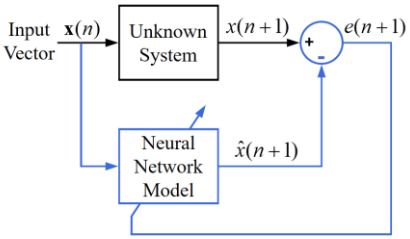

Figure 5. Block diagram of time series prediction using the NN model.

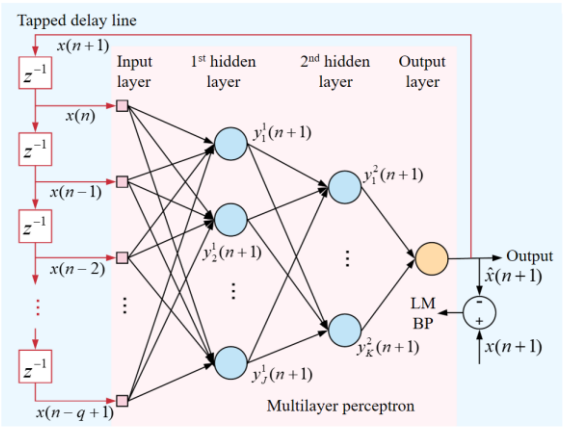

Figure 6. Architectural graph of a NAR network.

input layer of the MLP via a tapped-delay-line memory of q units. The output is denoted by $x(n+1)$. The signal vector $\mathbf{x}(n)$ applied to the input layer of the MLP consists of the delayed values of the output, namely, $x(n)$, $x(n-1)$, ..., $x(n-q+1)$. The dynamic behavior of the NAR model is described by

$$x(n+1) = F(x(n), x(n-1), \ldots, x(n-q+1)) \quad (1)$$

where F is a nonlinear function of its arguments. The MLP is used to approximate the function F. The dimension and values of the input vector $\mathbf{x}(n)$ should be determined, which are described in the next subsection. In Fig. 6, each circle represents a neuron. The model of each neuron in the 1st, 2nd, and output layers can be expressed as

$$y_j^1(n+1) = \varphi\left(b_j^1(n+1)+\boldsymbol{\omega}_j^1(n+1)\mathbf{x}(n)\right) \quad (2a)$$

$$y_k^2(n+1) = \varphi\left(b_k^2(n+1)+\boldsymbol{\omega}_k^2(n+1)\mathbf{y}^1(n+1)\right) \quad (2b)$$

$$\hat{x}(n+1) = \varphi(b^o(n+1)+\boldsymbol{\omega}^o(n+1)\mathbf{y}^2(n+1)) \quad (2c)$$

where $\varphi(v)$ is a nonlinear activation function. Here, a logistic function given by $\varphi(v) = \frac{1}{1+\exp(-av)}$ is used. Value a is an adjustable positive parameter. Also, $\boldsymbol{\omega}_j^1(n+1)$ and $b_j^1(n+1)$ are the weight vector and bias for the j^{th} hidden node in the 1st layer, $\boldsymbol{\omega}_k^2(n+1)$ and $b_k^2(n+1)$ are the weight vector and bias for the k^{th} hidden node in the 2nd layer, and $\boldsymbol{\omega}^o(n+1)$ and $b^o(n+1)$ are the weight vector and bias for the node in the output layer. Vector $\mathbf{y}^1(n+1)$ consists of all node outputs in the first layer (i.e. $y_j^1(n+1)$, $j = 1, 2, \ldots, J$), and $\mathbf{y}^2(n+1)$ consists of all node outputs in the second layer (i.e. $y_k^2(n+1)$, $k = 1, 2, \ldots, K$).

The error between the predicted time series $\hat{x}$(n+1) and the expected time series x(n+1) will be used for backward computation. The Levenberg-Marquardt backpropagation (LM BP) algorithm is employed as the training function to attain the fastest backpropagation performance.

The NAR network is trained to model the unknown system by using an open-loop NAR configuration. The trained network then is then switched to a closed-loop NAR configuration for multi-step-ahead prediction so that various delays can be implemented. By using the closed-loop mode, the NN can continue to predict by using internal feedback and simulate for as many predictions into the future as are desired.

B. Dynamic reconstruction

To identify the mapping that provides the NAR model, dynamic reconstruction is needed. A fundamental result in dynamic reconstruction theory is the delay embedding theorem developed by Takens [18], which shows that dynamic reconstruction is possible using the m-dimensional vector $\mathbf{x}(n)$ when given the observable $x(n+1)$. The vector $\mathbf{x}(n)$ is the input vector to the input layer and can be expressed as

$$\mathbf{x}(n) = [x(n), x(n-d), \ldots, x(n-(m-1)d)]^T \quad (3)$$

where m is the embedding dimension, and d is the normalized embedding delay.

To estimate the embedding dimension m, the method of false nearest neighbors is used. By increasing m, the fraction of the false neighbors will reduce, and an appropriate embedding dimension can be determined. For the fixed and varying rate and amplitude data, the explored embedding dimensions are chosen to be 18 and 25, respectively.

The proper prescription for choosing d is to recognize that the normalized embedding delay should be large enough for $x(n)$ and $x(n-d)$ to be essentially independent of each other, but not so independent as to have no correlation with each other. This can be achieved by using the d for which the mutual information between $x(n)$ and $x(n-d)$ attains its first minimum. The explored normalized embedding delays for fixed and varying rate and amplitude data are both selected to be 2.

Once the m and d are determined, the delayed inputs of the MLP $\mathbf{x}(n)$ can be determined. Each vector $\mathbf{x}(n)$ represents a point in the reconstructed state space which contains all necessary information to find the future points in the system's trajectory through state space.

C. Evaluations

To evaluate the prediction results, two evaluations are chosen: root-mean-square error (RMSE) and mean absolute error (MAE), which are expressed as

$$\text{RMSE} = \sqrt{\frac{\sum_{i=1}^{N}\left(x(n_i) - \hat{x}(n_i)\right)^2}{N}}, \quad \text{MAE} = \frac{\sum_{i=1}^{N}|x(n_i) - \hat{x}(n_i)|}{N} \quad (4)$$

where $x(n_i)$ is the desired output, $\hat{x}(n_i)$ is the actual prediction.

RMSE is a frequently used measure of the differences between values predicted by a model and the values observed; that is, it is a good measure of accuracy. MAE is well suited to compare prediction methods on a single series. Therefore, the RMSE will be used for the training data to explore the NN parameters (i.e. hidden layers # and neurons # in each layer) of the NAR from 12 architecture forms (Table I) by using fivefold cross-validation design. Then, both evaluations will be used for the testing data to evaluate the prediction results.

IV. RESULTS

The aim of this study is to demonstrate the effect of the NN-based heart motion prediction algorithm. Two types of datasets (dataset 1-5: fixed heart rate and maximum amplitude, and dataset 6-10: varying heart rate and maximum amplitude) are acquired and tested. Various prediction horizons are tested to explore the prediction ability of the method. The designed NN algorithm is compared to the EKF algorithm to verify the effectiveness of the proposed method.

A. The Effect of the NN Architecture

TABLE I. NEURON NETWORK ARCHITECTURE DESIGN

No.	Architecture	No.	Architecture	No.	Architecture
1	A-6-0-B	**5**	A-10-0-B	**9**	A-14-0-B
2	A-6-3-B	**6**	A-10-3-B	**10**	A-14-3-B
3	A-6-6-B	**7**	A-10-6-B	**11**	A-14-0-B
4	A-6-9-B	**8**	A-10-9-B	**12**	A-14-3-B

*The NN architecture form indicates the number of neurons in each layer. Here, A indicates the input number which is 18 for dataset 1-5 and 25 for dataset 6-10, and B indicates the output number which is 1.

Based on the design and methodology of the NAR network, for each architecture form, the RMSE across all five folds of cross-validation on each dataset is calculated and the mean and standard deviation across all ten datasets are presented in Fig. 7. It is seen that with more complex NN architecture, the RMSE becomes smaller. Also, due to the increase in complexity of the NN architecture, the computational capacity and the risk of overfitting increase. Considering this tradeoff, the explored NN architectures for dataset 1-5 (Fig. 7a) and dataset 6-10 (Fig. 7b) are chosen to be 18-10-6-1 and 25-10-9-1, respectively. The summarized architecture layouts of the NAR for the two types of datasets are shown in Fig. 8.

B. Experimental Results

By changing the delay length D in Fig. 8, various prediction horizons have tested. The time delay caused by US image acquisition and processing is approximately 160 ms [6]. As the frequency of the US machine is 25 Hz, the interval between two data points is 40 ms. Therefore, to compensate for a delay of 160 ms, 4 steps ahead should be predicted. In Fig. 9, the NN-based prediction results of a ten-second fixed rate and maximum amplitude data are presented and compared to the actual tracked POI position data. The prediction results using an EKF algorithm [4] are also presented in Fig. 9. The EKF takes advantage of the quasi-periodicity of the heart motion that is modeled as a time-varying Fourier series to compensate for the time delay. The EKF is tested with the same POI position data and compared to the results of the NN predictor. The reported errors between the predicted and the actual tracked POI position data in Fig. 9 show that the NN prediction results are better than the EKF prediction results.

Furthermore, the NN and EKF predictors are tested for all datasets. The means and standard deviations of the two evaluations are listed in Table II. For dataset 1-5, both MAE and RMSE using NN are lower than those of using EKF with

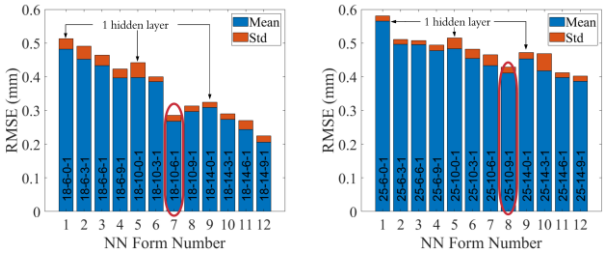

(a) (b)

Figure 7. The RMSE results of the designed different NN architecture forms for (a) dataset 1-5 and (b) dataset 6-10.

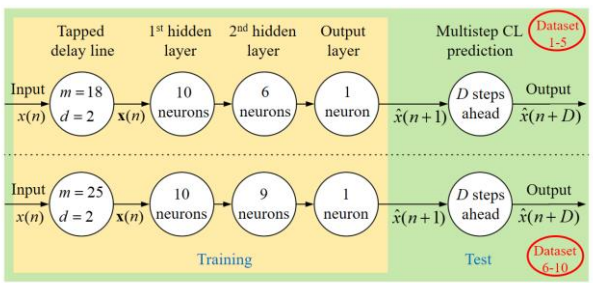

Figure 8. The architectural layout of the designed NAR network.

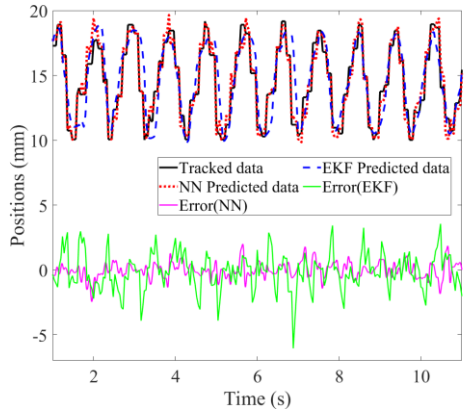

Figure 9. The heart motion prediction results with a time delay of 160 ms.

TABLE II. EVALUATIONS FOR A DELAY OF 160 MS

Dataset	Algorithm	MAE (mm)	RMSE (mm)
1-5	NN	0.3757 ± 0.0536	0.5177 ± 0.0842
	EKF	0.9592 ± 0.0245	1.3442 ± 0.0346
6-10	NN	0.6305 ± 0.0440	0.7411 ± 0.0664
	EKF	1.9540 ± 0.1384	2.5871 ± 0.1176

reduction by 60%, while for dataset 6-10, the two evaluations using NN are roughly 70% less than those of using EKF.

To further explore the prediction performance of the two algorithms with respect to different datasets and time delays, the prediction horizon *D* is changed from 1 to 8 consecutively, which means the delay is changing from 40 ms to 320 ms with an interval of 40 ms. The means and standard deviations of MAE and RMSE for two types of datasets are shown in Fig. 10. It is seen that the NN prediction has much lower errors

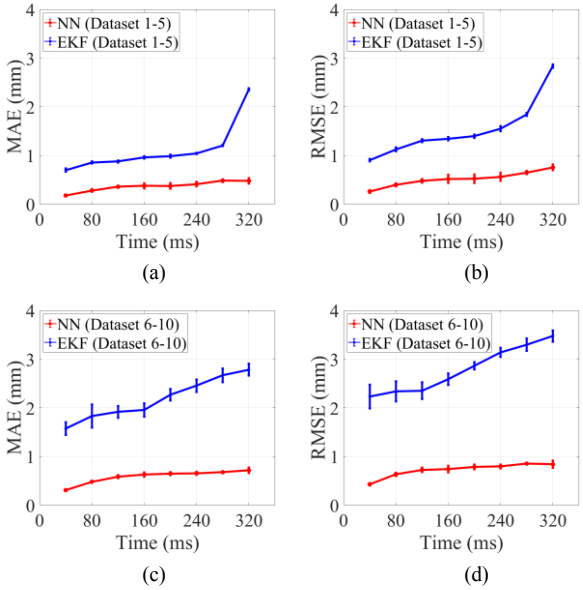

(a) (b)

(c) (d)

Figure 10. The MAE and RMSE in heart motion prediction for time delays that are changed from 40 ms to 320 ms with an interval of 40 ms, using NN and EKF. (a) and (b) are the MAE and RMSE for dataset 1-5, while (c) and (d) are the MAE and RMSE for dataset 6-10.

compared to the EKF prediction, regardless of the types of the datasets, the evaluations, and the delayed time.

The NN algorithm is applied to both types of datasets to measure the prediction ability of the POI position up to 1000 ms in advance. Fig. 11 shows the prediction performance using NN for time delays of 200, 400, 600, 800, and 1000 ms. Both MAE and RMSE increase as the delayed time increases. The prediction for the varying rate and maximum amplitude datasets (dataset 6-10) has higher errors compared to those for the fixed rate and maximum amplitude datasets (dataset 1-5). For dataset 6-10, the prediction accuracy using NN for delay of 1000 ms is like that of using EKF for delay of 40 ms (Fig. 10c and 10d). This demonstrates that the NN algorithm presents significant advantages over the EKF algorithm such as higher accuracy and longer prediction horizon.

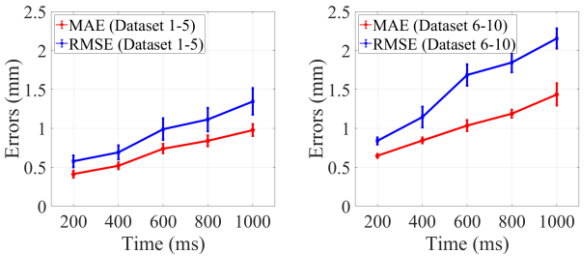

(a) (b)

Figure 11. The MAE and RMSE in POI position prediction for (a) dataset 1-5 and (b) 6-10 for delays of 200, 400, 600, 800, and 1000 ms, using NN.

V. Conclusion

A method of heart motion prediction was proposed to compensate for the non-negligible time delays caused by ultrasound image acquisition and processing. A nonlinear autoregressive network was used to solve the prediction problem for the datasets that consist of fixed and varying heart rate and maximum amplitude data. The neural network algorithm was compared to an extended Kalman filter algorithm. Using neural network, mean absolute error and the root mean squared error decreased significantly compared to those of using extended Kalman filter. Also, the neural network algorithm was proved to be able to predict the heart position up to 1000 ms in advance. The results showed that the neural network algorithm has higher accuracy and prediction ability than the extended Kalman filter algorithm, which makes it possible for the neural network algorithm to be used in robotics-assisted beating-heart surgery. Future work will involve combining the designed neural network algorithm with the telerobotic system for beating-heart surgery to compensate for the beating heart's motion so that specific tasks can be operated on the beating-heart tissue.

Acknowledgement

Research supported by the Canada Foundation for Innovation (CFI) under grant LOF 28241 and JELF 35916, the Alberta Innovation and Advanced Education Ministry under Small Equipment Grant RCP-12-021, the Alberta Innovation and Advanced Education Ministry under Small Equipment Grant RCP-17-019, the Natural Sciences and Engineering Research Council (NSERC) of Canada under grant RGPIN 372042, the Natural Sciences and Engineering Research Council (NSERC) of Canada under grant RGPIN 03907, and the China Scholarship Council (CSC) under grant [2015]08410152.

Reference

[1] Y. Nakamura, K. Kishi, and H. Kawakami, "Heartbeat synchronization for robotic cardiac surgery," *Proc. - IEEE Int. Conf. Robot. Autom.*, vol. 2, pp. 2014–2019, 2001.

[2] D. T. Kettler, R. D. Plowes, P. M. Novotny, N. V. Vasilyev, P. J. Del Nido, and R. D. Howe, "An active motion compensation instrument for beating heart mitral valve surgery," in *IEEE International Conference on Intelligent Robots and Systems*, 2007, no. October, pp. 1290–1295.

[3] L. Cheng, M. Sharifi, and M. Tavakoli, "Towards robot-assisted anchor deployment in beating-heart mitral valve surgery," *Int. J. Med. Robot. Comput. Assist. Surg.*, vol. 14, no. 3, pp. 1–10, 2018.

[4] L. Cheng and M. Tavakoli, "Ultrasound image guidance and robot impedance control for beating-heart surgery," *Control Eng. Pract.*, vol. 81, pp. 9–17, 2018.

[5] L. Cheng and M. Tavakoli, "Switched-Impedance Control of Surgical Robots in Teleoperated Beating-Heart Surgery," *J. Med. Robot. Res.*, pp. 1841003, 2018.

[6] M. Bowthorpe and M. Tavakoli, "Generalized Predictive Control of a Surgical Robot for Beating-Heart Surgery Under Delayed and Slowly-Sampled Ultrasound Image Data," *IEEE Robot. Autom. Lett.*, vol. 1, no. 2, pp. 892–899, 2016.

[7] S. G. Yuen, D. P. Perrin, N. V Vasilyev, P. J. Nido, R. D. Howe, and S. Member, "Force Tracking With Feed-Forward Motion Estimation for Beating Heart Surgery," *IEEE Trans. Robot.*, vol. 26, no. 5, pp. 888–896, 2010.

[8] R. Cortesão and M. Dominici, "Robot Force Control on a Beating Heart," *IEEE/ASME Trans. Mechatronics*, vol. 22, no. 4, pp. 1736–1743, 2017.

[9] N. Hogan, "Impedance Control: An Approach to Manipulation : Part I — Theory," *ASME, J. Dyn. Syst. Meas. Control*, vol. 107(1), pp. 1–7, 1985.

[10] S. B. Kesner and R. D. Howe, "Robotic catheter cardiac ablation combining ultrasound guidance and force control," *Int. J. Rob. Res.*, vol. 33, no. 4, pp. 631–644, 2014.

[11] B. Doucoure, K. Agbossou, and A. Cardenas, "Time series prediction using arti fi cial wavelet neural network and multi-resolution analysis : Application to wind speed data," *Renew. Energy*, vol. 92, pp. 202–211, 2016.

[12] J. Tang, F. Liu, Y. Zou, W. Zhang, and Y. Wang, "An Improved Fuzzy Neural Network for Traffic Speed Prediction Considering," vol. 18, no. 9, pp. 2340–2350, 2017.

[13] L. Guo, N. Li, F. Jia, Y. Lei, and J. Lin, "Neurocomputing A recurrent neural network based health indicator for remaining useful life prediction of bearings," *Neurocomputing*, vol. 240, pp. 98–109, 2017.

[14] I. Bukovsky *et al.*, "A Fast Neural Network Approach to Predict Lung Tumor Motion during Respiration for Radiation Therapy Applications," *Biomed Res. Int.*, p. 489679(1-13), 2015.

[15] T. P. Teo *et al.*, "Feasibility of predicting tumor motion using online data acquired during treatment and a generalized neural network optimized with of fl ine patient tumor trajectories," *Am. Assoc. Phys. Med.*, vol. 45, no. 2, pp. 830–845, 2018.

[16] V. De Luca *et al.*, "Evaluation of 2D and 3D ultrasound tracking algorithms and impact on ultrasound-guided liver radiotherapy margins," *Am. Assoc. Phys. Med.*, vol. 45, no. 11, pp. 4986–5003, 2018.

[17] M. Bowthorpe, V. Castonguay-siu, and M. Tavakoli, "Development of a Robotic System to Enable Beating-heart Surgery," *J. Robot. Soc. Japan*, vol. 32, no. 4, pp. 23–30, 2014.

[18] F. Takens, "On the numerical determinationof the dimension of an attractor," *Dynamical systems and bifurcations*, Springer, Berlin, Heidelberg, pp. 99-106, 1985.